A limited role of NKCC1 in telencephalic glutamatergic neurons for developing hippocampal network dynamics and behavior

Jürgen Graf[a,1], Chuanqiang Zhang[a,1,2], Stephan Lawrence Marguet[b,c,1], Tanja Herrmann[d,1], Tom Flossmann[a,3], Robin Hinsch[b,c], Vahid Rahmati[e], Madlen Guenther[a], Christiane Frahm[a], Anja Urbach[a], Ricardo Melo Neves[b,c], Otto W. Witte[a], Stefan J. Kiebel[e], Dirk Isbrandt[b,c], Christian A. Hübner[d], Knut Holthoff[a,4], and Knut Kirmse[a,f,4,5]

[a]Hans-Berger Department of Neurology, Jena University Hospital, 07747 Jena, Germany; [b]Institute for Molecular and Behavioral Neuroscience, University of Cologne, 50937 Cologne, Germany; [c]Experimental Neurophysiology, German Center for Neurodegenerative Diseases, 53127 Bonn, Germany; [d]Institute of Human Genetics, Jena University Hospital, 07747 Jena, Germany; [e]Department of Psychology, Technical University Dresden, 01187 Dresden, Germany; and [f]Department of Neurophysiology, Institute of Physiology, University of Würzburg, 97070 Würzburg, Germany

Edited by Lily Yeh Jan, University of California, San Francisco, CA, and approved February 22, 2021 (received for review July 14, 2020)

NKCC1 is the primary transporter mediating chloride uptake in immature principal neurons, but its role in the development of in vivo network dynamics and cognitive abilities remains unknown. Here, we address the function of NKCC1 in developing mice using electrophysiological, optical, and behavioral approaches. We report that NKCC1 deletion from telencephalic glutamatergic neurons decreases in vitro excitatory actions of γ-aminobutyric acid (GABA) and impairs neuronal synchrony in neonatal hippocampal brain slices. In vivo, it has a minor impact on correlated spontaneous activity in the hippocampus and does not affect network activity in the intact visual cortex. Moreover, long-term effects of the developmental NKCC1 deletion on synaptic maturation, network dynamics, and behavioral performance are subtle. Our data reveal a neural network function of NKCC1 in hippocampal glutamatergic neurons in vivo, but challenge the hypothesis that NKCC1 is essential for major aspects of hippocampal development.

GABA | NKCC1 | hippocampus | development | in vivo

Intracellular chloride concentration ($[Cl^-]_i$) is a major determinant of neuronal excitability, as synaptic inhibition is primarily mediated by chloride-permeable receptors (1). In the mature brain, $[Cl^-]_i$ is maintained at low levels by chloride extrusion, which renders γ-aminobutyric acid (GABA) hyperpolarizing (2) and counteracts activity-dependent chloride loads (3). GABAergic inhibition in the adult is crucial not only for preventing runaway excitation of glutamatergic cells (4) but also for entraining neuronal assemblies into oscillations underlying cognitive processing (5). However, the capacity of chloride extrusion is low during early brain development (6, 7). Additionally, immature neurons are equipped with chloride uptake mechanisms, particularly with the $Na^+/K^+/2Cl^-$ cotransporter NKCC1 (8–12). NKCC1 contributes to the maintenance of high $[Cl^-]_i$ in the developing brain (13), favoring depolarization through $GABA_A$ receptor ($GABA_AR$) activation in vivo (14, 15).

When GABA acts as a depolarizing neurotransmitter, neural circuits generate burst-like spontaneous activity (16–20), which is crucial for their developmental refinement (21–24). In vitro evidence indicates that GABAergic interneurons promote neuronal synchrony in an NKCC1-dependent manner (10, 12, 25–28). However, the in vivo developmental functions of NKCC1 are far from understood (29, 30). One fundamental question is to what extent NKCC1 and GABAergic depolarization supports correlated spontaneous activity in the neonatal brain. In the neocortex, GABA imposes spatiotemporal inhibition on network activity already in the neonatal period (14, 25, 31, 32). Whether a similar situation applies to other brain regions is unknown, as two recent chemo- and optogenetic studies in the hippocampus yielded opposing results (25, 33). Manipulations of the chloride driving force are potentially suited to resolve these divergent findings, but pharmacological (34–36) or conventional knockout (10, 11, 37) strategies suffer from unspecific effects that complicate interpretations.

Here, we overcome this limitation by selectively deleting *Slc12a2* (encoding NKCC1) from telencephalic glutamatergic neurons. We show that chloride uptake via NKCC1 promotes synchronized activity in acute hippocampal slices, but has weak and event type-dependent effects in CA1 in vivo. Long-term loss of NKCC1 leads to subtle changes of network dynamics in the adult, leaving synaptic development unperturbed and behavioral performance intact. Our data suggest that NKCC1-dependent chloride

Significance

Neuronal circuits develop in an activity-dependent manner. In vitro data suggest that the intracellular accumulation of chloride—a universal characteristic of immature nerve cells—drives network maturation through a depolarizing action of the neurotransmitter GABA. We here demonstrate that deletion of the chloride cotransporter NKCC1 from forebrain pyramidal cells severely impairs hippocampal network synchrony in vitro. In contrast, NKCC1 has weak and event type-dependent effects on spontaneous network activity in vivo, and loss of NKCC1 leaves the maturation of synaptic properties, network dynamics, and hippocampus-dependent behaviors largely unaffected. Our data reveal a subtle neural network function of NKCC1 in hippocampal glutamatergic neurons in vivo, but challenge the assertion that NKCC1 in this major cell type is central to hippocampal development.

Author contributions: S.J.K., D.I., C.A.H., K.H., and K.K. designed research; J.G., C.Z., S.L.M., T.H., T.F., R.H., M.G., and K.K. performed research; J.G., C.Z., S.L.M., T.H., T.F., V.R., M.G., C.F., A.U., R.M.N., D.I., and K.K. analyzed data; and J.G., C.Z., S.L.M., T.H., T.F., V.R., M.G., C.F., A.U., R.M.N., O.W.W., S.J.K., D.I., C.A.H., K.H., and K.K. wrote the paper.

The authors declare no competing interest.

This article is a PNAS Direct Submission.

[1]J.G., C.Z., S.L.M., and T.H. contributed equally to this work.

[2]Present address: Laboratory of Sensory Processing, Brain Mind Institute, Faculty of Life Sciences, École Polytechnique Fédérale de Lausanne, CH-1015 Lausanne, Switzerland.

[3]Present address: Centre for Discovery Brain Sciences, Biomedical Sciences, University of Edinburgh, EH8 9XD Edinburgh, United Kingdom.

[4]K.H. and K.K. contributed equally to this work.

[5]To whom correspondence may be addressed. Email: knut.kirmse@uni-wuerzburg.de.

This article contains supporting information online at https://www.pnas.org/lookup/suppl/doi:10.1073/pnas.2014784118/-/DCSupplemental.

Published March 29, 2021.

uptake is largely dispensable for several key aspects of hippocampal development in vivo.

Results

Behavioral Performance of Mice in the Conditional Absence of NKCC1 from Telencephalic Glutamatergic Cells. To investigate the role of depolarizing GABA in telencephalic glutamatergic neurons, we deleted *Slc12a2* in *Emx1*-lineage cells of embryonic mice (Fig. 1*A*). A comparison with *NKCC1*$^{flox/flox}$ (wild-type [WT]) littermates showed that Cre-dependent recombination had been widespread in the hippocampus (Fig. 1*B*) and profoundly reduced hippocampal *Slc12a2* mRNA levels in *Emx1*^{IREScre}:*NKCC1*$^{flox/flox}$ (KO^{Emx1}) mice at postnatal days (P) 2 to 3 (Fig. 1*C* and *SI Appendix*, Table S1). Fate mapping of *Emx1*-lineage cells at P54 to 63 confirmed that Cre expression was restricted to glutamatergic neurons (GAD67^{-}/NeuN^{+}), whereas cells expressing a pan-GABAergic (GAD67) or subtype-selective GABAergic interneuron (parvalbumin or somatostatin) marker were reporter negative (*SI Appendix*, Fig. S1 *A–J*). WT and KO^{Emx1} mice were born at Mendelian ratios ($P = 0.41$, $\chi^2 = 0.69$, $n = 71$ mice, χ^2 test), displayed a normal postnatal gain in body weight (*SI Appendix*, Fig. S1*K*), similar brain growth (measured by lambda-bregma distance, *SI Appendix*, #S14

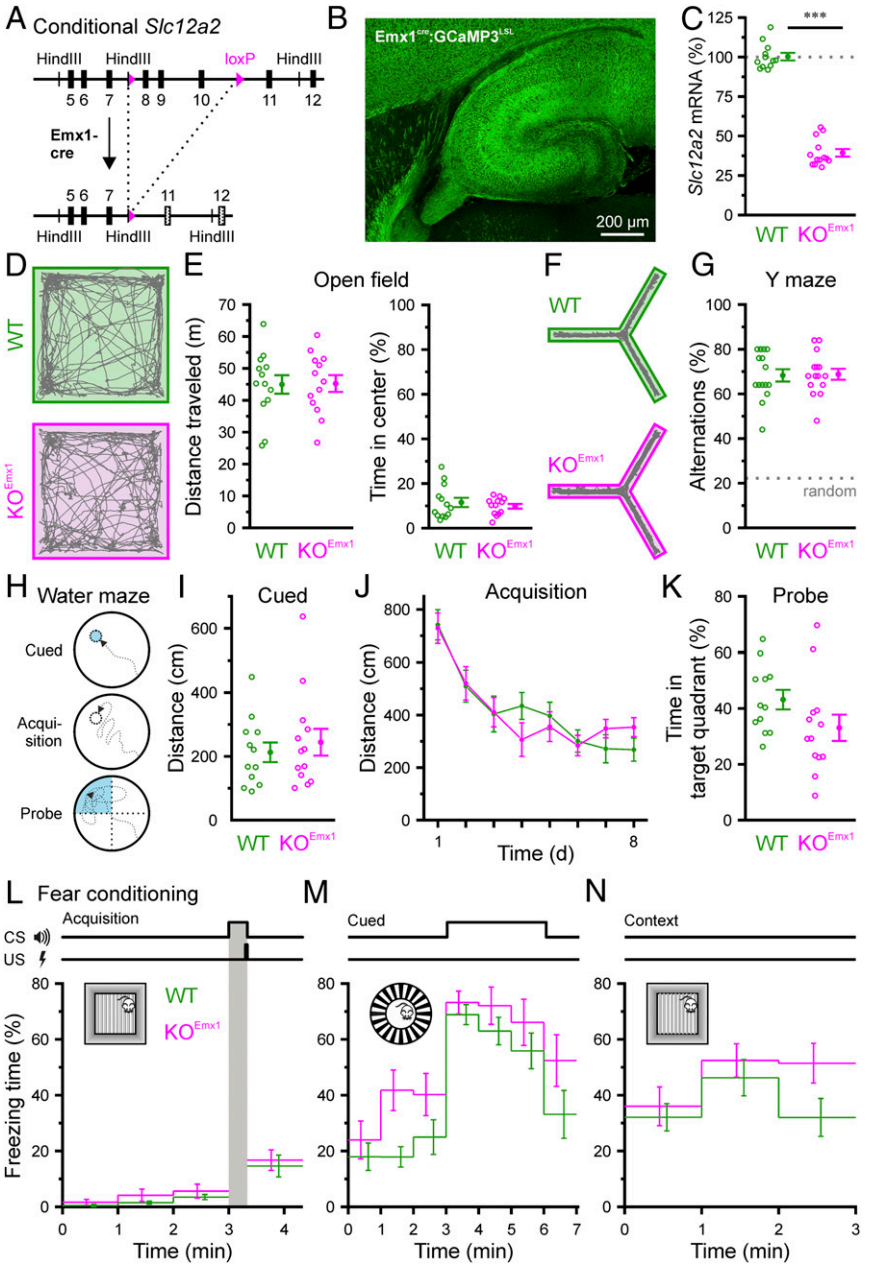

Fig. 1. Behavioral performance of NKCC1 KO^{Emx1} mice. (*A*) In the targeted *Slc12a2* locus, exons 8 to 10 are flanked by loxP sites. Cre-dependent recombination causes a frameshift (dotted) and introduces a stop codon in exon 12. (*B*) Confocal image demonstrating Cre-reporter expression (GCaMP3) in a horizontal brain slice (P4). (*C*) Hippocampal *Slc12a2* mRNA levels compared with the geometric mean of WT, normalized to *Gapdh* and *Hmbs*. (*D*) Sample trajectories in the open field. (*E*) Total distance covered and relative time spent in the center. (*F*) Sample trajectories in the Y maze. (*G*) Spontaneous alternations (dotted, chance level). (*H*) Morris water maze. (*I* and *J*) Distance to platform for cued trial (visible platform) and acquisition (hidden platform). (*K*) Time in target quadrant during probe trial (no platform). (*L–N*) Freezing time during fear conditioning (*L*), reexposure to cue (*M*), and context (*N*). (*C–K*) Open circles represent single animals. (*E–N*) Mean ± SEM; CS, conditioned stimulus; US, unconditioned stimulus; ***$P < 0.001$. See *SI Appendix*, Fig. S1 and Table S1.

in Table S1), and unperturbed developmental reflexes, including cliff avoidance behavior and righting reflex (*SI Appendix*, Fig. S1 *L* and *M*). Unlike conventional NKCC1 knockout mice (38), adult KO^{Emx1} mice exhibited unaltered locomotion and exploration in the open field (Fig. 1 *D* and *E*). Spontaneous alternations in a Y maze, a measure of spatial working memory, were unaffected (Fig. 1 *F* and *G*). Spatial learning and memory in a Morris water maze (Fig. 1 *H*–*K*), as well as cue- and context-specific fear memory (Fig. 1 *L*–*N*), were not significantly altered either. In sum, KO^{Emx1} mice lack the severe phenotype of NKCC1 null mice, which is due to NKCC1 loss from tissues other than the brain (37), and display a normal development of several hippocampus-dependent and -independent behaviors.

Loss of NKCC1 Attenuates the Depolarizing Action of GABA. To investigate how $NKCC1^{Emx1}$ loss alters cellular GABA actions in the neonatal hippocampus, we used low-gramicidin perforated-patch current-clamp recordings that allow monitoring the membrane potential (V_m), while minimizing the risk of membrane breakthrough (39, 40). Measurements were performed in slices (P3 to 4) in the presence of antagonists of ionotropic glutamate receptors (10 μM 6,7-dinitroquinoxaline-2,3-dione [DNQX], 50 μM DL-2-amino-5-phosphonopentanoic acid [APV]) and voltage-gated Na^+ (0.5 μM tetrodotoxin [TTX]) and Ca^{2+} (100 μM $CdCl_2$) channels so as to block recurrent excitation and amplification of voltage changes by intrinsic conductances. Resting V_m of CA3 pyramidal cells (PCs) was similar in WT and KO^{Emx1} mice (Fig. 2 *A* and *B* and *SI Appendix*, Table S2). However, NKCC1 deletion significantly reduced the peak membrane potential (V_{peak}) induced by a saturating puff of the $GABA_AR$ agonist isoguvacine (100 μM, 2 s) by almost 10 mV (Fig. 2*B*). Because V_{peak} will approximate the reversal potential of $GABA_AR$-mediated currents (E_{GABA}) under these conditions, our data imply lower $[Cl^-]_i$ in NKCC1 KO^{Emx1} mice. Isoguvacine-induced V_m changes were consistent across trials (Fig. 2*C*). Moreover, amplitudes of somatic Ca^{2+} transients (CaTs) evoked by bath-applied GABA (100 μM) were attenuated in putative PCs of KO^{Emx1} mice (P2 to 4), whereas glutamate-induced CaTs were unaffected (*SI Appendix*, Fig. S2). Furthermore, cell-attached recordings in the presence of DNQX (10 μM) and APV (50 μM) revealed that puff-applied isoguvacine (100 μM) increased action potential (AP) frequency in WT, but not in KO^{Emx1}, mice at P3 to 4 (Fig. 2 *D*–*F*). We conclude that NKCC1 deletion attenuates $GABA_AR$-mediated depolarization and virtually abolishes excitatory GABA effects in vitro.

PC-Specific NKCC1 Deletion Impairs Spontaneous Hippocampal Network Activity In Vitro. Based on experimental and theoretical results (10, 27, 35), we hypothesized that a PC-specific attenuation of GABAergic depolarization would impair network synchrony. We tested this prediction in the CA3 of acute slices (P1 to 4) using whole-cell recordings of spontaneous GABAergic postsynaptic currents (sGPSCs) isolated by their reversal potential (Fig. 3*A*). sGPSC frequencies did not significantly differ between genotypes (Fig. 3*B* and *SI Appendix*, Table S3). In WT slices, sGPSCs typically occurred in bursts (known as giant depolarizing potentials [GDPs]) (41). However, this temporal structure was largely absent in cells from KO^{Emx1} mice. For quantification, a burst index was computed for measured data and compared with a Poisson point process in which sGPSCs occur randomly. Burst indices of WT, but not of KO^{Emx1} cells were consistently higher than those expected for a random case (Fig. 3*C*). Controlling for the effect of sGPSC frequency, we found that burst indices were significantly reduced by $NKCC1^{Emx1}$ loss (Fig. 3*D*), indicating impaired neuronal synchrony. This conclusion was confirmed by single-cell confocal Ca^{2+} imaging revealing a dramatic reduction in GDP frequency in CA3 of KO^{Emx1} mice at P1 to 4 (*SI Appendix*, Fig. S3). Of note, the effects of $NKCC1^{Emx1}$ loss were region dependent because the kinetics of single-cell recruitment in CA1 during GDPs was significantly slowed down in KO^{Emx1} mice, while GDP frequency was similar (*SI Appendix*, Fig. S3).

In large-scale confocal Ca^{2+} imaging experiments (GCaMP3^{Emx1}) at P1 to 4, large-amplitude network events were detected in slices from WT (*Emx1^{IREScre}:NKCC1$^{wt/wt}$:GCaMP3^{LSL}*) mice, often involving multiple hippocampal subfields and/or both hippocampal and adjacent cortical areas (Fig. 3*E*). When CA1 was coactive, it stereotypically followed activity in CA3 or the medial entorhinal cortex (*SI Appendix*, Fig. S4). While large-scale activity was also present in KO^{Emx1} (*Emx1^{IREScre}:NKCC1$^{flox/flox}$:GCaMP3^{LSL}*) slices, the area under the curve of network events

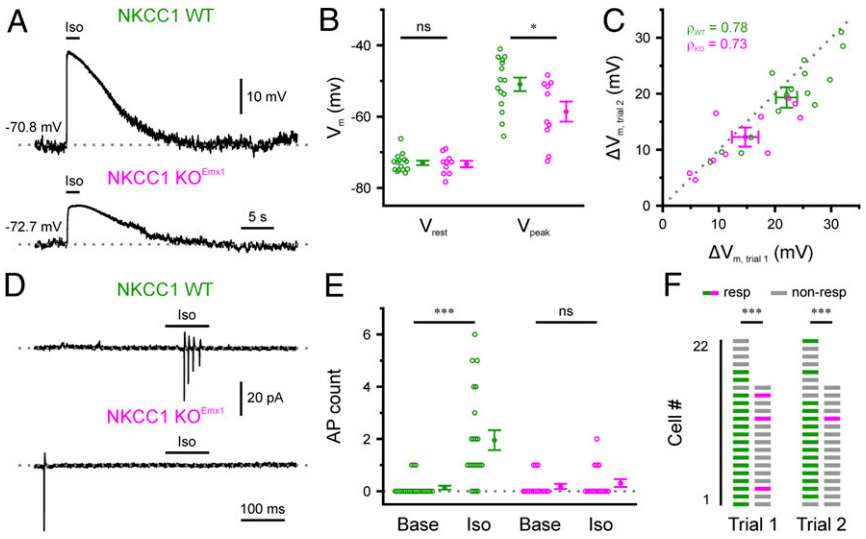

Fig. 2. Loss of NKCC1 attenuates the depolarizing action of GABA. (*A*) Sample gramicidin perforated-patch current-clamp recordings in response to puff-applied isoguvacine (Iso). (*B*) Resting (V_{rest}) and peak isoguvacine-induced (V_{peak}) membrane potential. (*C*) Correlation of isoguvacine-induced membrane potential changes (ΔV_m) in two successive trials. ρ, Spearman's rank correlation coefficient. (*D*) Sample cell-attached recordings in response to puff-applied isoguvacine. (*E*) Number of action currents (300-ms intervals) immediately before (base) and after (Iso) puff onset. (*F*) Reduced fraction of responsive cells (resp) in KO^{Emx1} mice. Open circles represent single cells. Mean ± SEM; ns, not significant; $*P < 0.05$, $***P < 0.001$. See *SI Appendix*, Fig. S2 and Table S2.

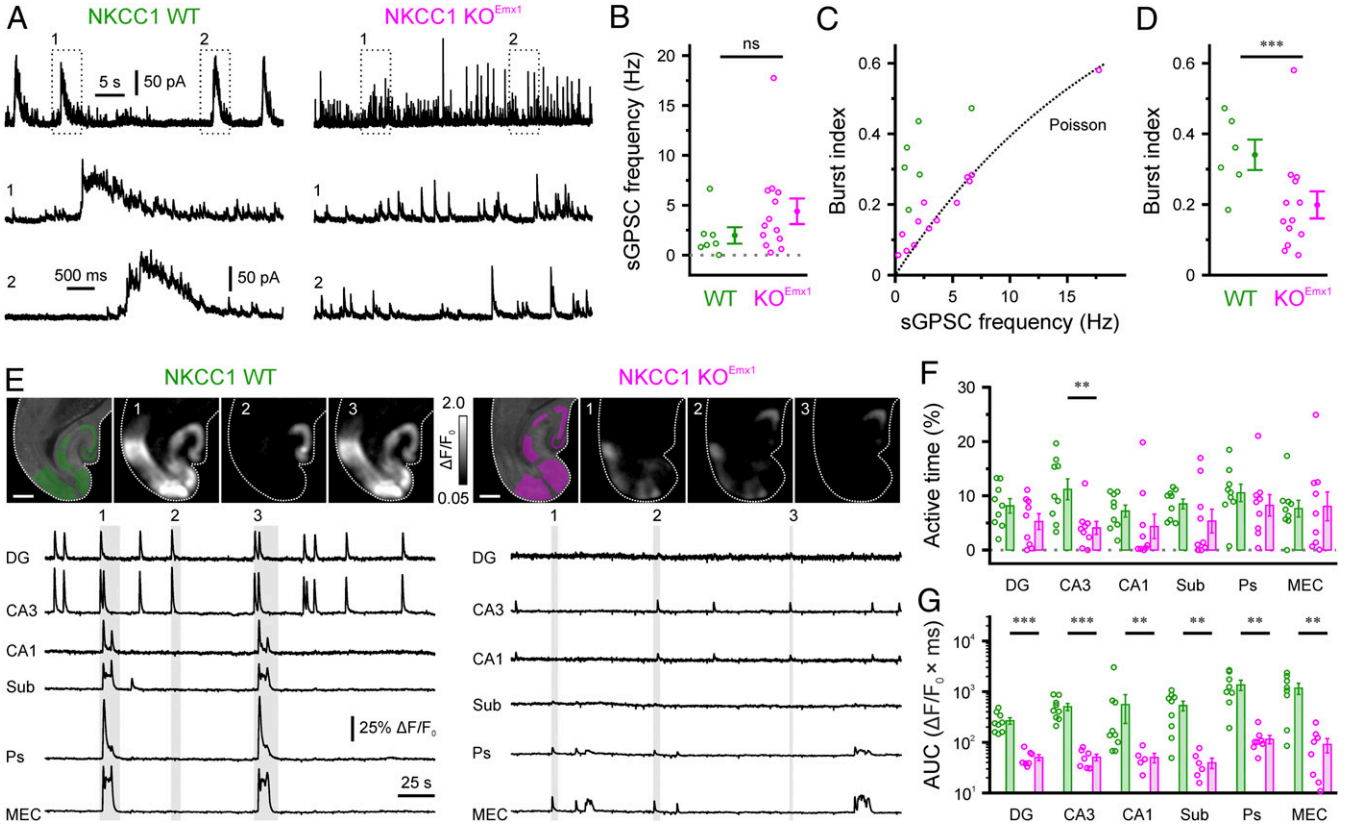

Fig. 3. NKCC1^{Emx1} deletion impairs spontaneous hippocampal activity in vitro. (*A*) Sample whole-cell recordings of sGPSCs isolated by reversal potential. (*B*) sGPSC frequency. (*C*) Burst index vs. sGPSC frequency. The dotted line represents a Poisson point process. (*D*) Burst indices. (*E*) GCaMP-based confocal imaging of spontaneous activity in corticohippocampal slices. *Top*: GCaMP3 fluorescence overlaid with ROIs for analysis (*Left*) and sample $\Delta F/F_0$ images for time periods indicated below. (Scale bars, 500 μm.) *Bottom*: $\Delta F/F_0$ sample traces. (*F* and *G*) Total active time (*F*) and mean area under the curve per event (AUC, *G*). Open circles represent single cells (*B–D*) or slices (*F* and *G*). Mean ± SEM; ns, not significant; $^*P < 0.05$, $^{**}P < 0.01$, $^{***}P < 0.001$. See *SI Appendix*, Figs. S3 and S4 and Table S3.

was substantially reduced (Fig. 3*G*). Additionally, a reduced active time was found in CA3 (Fig. 3*F*). We thus conclude that PC-specific NKCC1 deletion leads to a profound attenuation of neuronal synchrony in vitro.

NKCC1 Effects on Network Dynamics Are Not Accounted for by Alterations in Intrinsic Excitability or Basic Synaptic Properties. The question of how GABA instructs neurodevelopment remains largely unanswered (29). Some data indicate that a lack of NKCC1 interferes with the normal maturation of synaptic (9) or intrinsic (11) conductances. We therefore examined whether altered network dynamics in NKCC1 KO^{Emx1} mice reflect an acute shift in E_{GABA} or developmental changes following NKCC1 disruption in embryonic life. As an overall measure of intrinsic excitability, we first assessed spontaneous AP firing in the presence of synaptic receptor antagonists (10 μM DNQX, 50 μM APV, 10 μM bicuculline methiodide [BMI]) using cell-attached recordings from CA3 PCs (P3 to 4). In contrast to results from NKCC1 null mice (11), AP frequencies were unaffected by conditional NKCC1 loss (Fig. 4 *A* and *B* and *SI Appendix*, Table S4). Moreover, NKCC1^{Emx1} disruption did not significantly alter neuronal input–output relationships (Fig. 4 *C* and *D*). Accordingly, passive membrane properties (*SI Appendix*, #S10–S12 in Table S4) and AP threshold (Fig. 4*E*) were unaffected.

We next investigated whether basic properties of glutamatergic/GABAergic synapses were altered upon NKCC1^{Emx1} disruption. Whole-cell recordings from CA3 PCs were performed at P3 to 4 and P14 to 16, covering a time period of intense synaptogenesis and subunit reorganization of postsynaptic receptors. AMPA receptor-dependent miniature PSCs (mEPSCs) displayed a profound developmental increase in frequency, accompanied by an increase in (quantal) amplitude and a deceleration in decay kinetics (Fig. 4 *F* and *G*) (42). These alterations were independent of genotype (*SI Appendix*, #S4–S6, Table S4). $GABA_A$R-mediated miniature postsynaptic currents (mGPSCs) also underwent a substantial developmental increase in frequency (Fig. 4 *H* and *I*, *Left*), along with an acceleration in their decay kinetics (Fig. 4 *I*, *Right*) (43), but no change in quantal amplitude (Fig. 4 *I*, *Middle*). These developmental trajectories were indistinguishable between WT and KO^{Emx1} mice (*SI Appendix*, #S7–S9, Table S4). In summary, both intrinsic excitability and basic synaptic properties were unaffected by NKCC1^{Emx1} loss and, thus, are unlikely to account for the alteration of in vitro hippocampal network dynamics in KO^{Emx1} mice.

Hippocampal Sharp Waves In Vivo Persist in the Conditional Absence of NKCC1. Next, we investigated the effect of NKCC1^{Emx1} deletion on in vivo hippocampal network multiunit activity (MUA) at P4. We recorded local field potentials (LFPs) along the CA1–dentate gyrus axis using linear 32-site silicon probes in awake head-fixed neonates. We observed similar activity patterns in P4 hippocampi of both WT and NKCC1 KO^{Emx1} mice: sharp waves (SPWs) with a phase reversal in CA1 stratum pyramidale (s.p.) and short-lasting oscillations in the 10 to 30 Hz (beta) frequency range (hippocampal network oscillations [HNOs]) (Fig. 5 *A* and *B*) (36, 44). Depth profiles of SPWs were comparable to those in

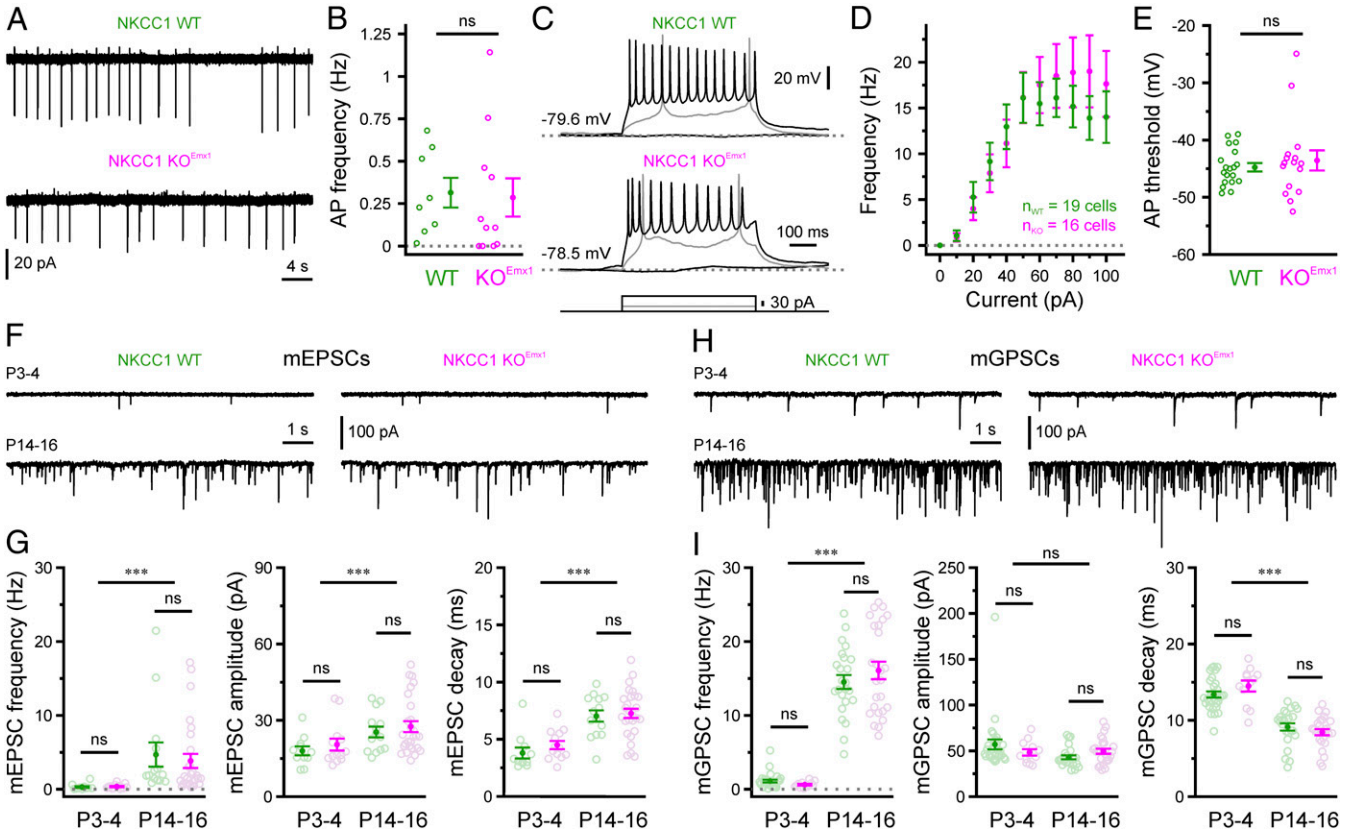

Fig. 4. NKCC1 effects on hippocampal network dynamics are not accounted for by alterations in intrinsic excitability or basic synaptic properties. (*A*) Sample cell-attached recordings in the presence of ionotropic glutamate and GABA receptor antagonists. (*B*) Mean spontaneous AP frequency. (*C*) Sample current-clamp recordings in response to current injections. (*D* and *E*) Current–frequency relationship (*D*) and AP threshold (*E*) are unaltered. (*F*) Sample voltage-clamp measurements of mEPSCs. (*G*) mEPSC frequency, median mEPSC amplitude, and mean mEPSC decay-time constant. (*H*) Sample voltage-clamp measurements of mGPSCs. (*I*) mGPSC frequency, median mGPSC amplitude and mean mGPSC decay-time constant. Open circles represent single cells. Mean ± SEM; ns, not significant; ***$P < 0.001$. See *SI Appendix*, Table S4.

rats (45) ("rad/lm SPW" in Fig. 5*C*). Additionally, we found inverted SPWs with their maximum current sink in stratum oriens (s.o.) ("oriens SPW" in Fig. 5*C*). Both SPW types elicited distinct MUA patterns in the CA1 pyramidal layer that were similar for both genotypes. None of these SPW event properties such as occurrence frequency, amplitudes, or event durations differed between WT and KO^{Emx1} animals (Fig. 5*D* and *SI Appendix*, Table S5). Likewise, SPW properties did not differ between genotypes at P7 or P12 (*SI Appendix*, Fig. S5). MUA counts in 50-ms bins either centered around, or aligned to, 0 ms for oriens and rad/lm SPWs, respectively, also did not differ by genotype (Fig. 5*D* and *SI Appendix*, Table S5). Furthermore, HNO rate and length were similar between the genotypes at P4 (Fig. 5*E*). HNO MUA shape was also comparable between genotypes, and MUA spike counts in the first 500-ms bin—although highly variable across animals—did not differ between WT and KO^{Emx1} mice (Fig. 5*E*).

NKCC1 Promotes In Vivo Correlated Network Activity in the Hippocampus, but Not in the Visual Cortex. We further characterized in vivo network dynamics using wide-field Ca^{2+} imaging, which primarily reflects AP firing and allows recording from a large field of view (FOV). For optical access to CA1 in vivo, a hippocampal window preparation (46) was adapted for use in neonatal mice (P3 to 4; Fig. 6*A*). LFP recordings using a tungsten electrode positioned in stratum radiatum (s.r.) confirmed that SPW frequencies measured through the intact cortex or after focal cortex aspiration did not differ significantly (*SI Appendix*, Fig. S6 *A–C* and Table S6). Ca^{2+} imaging was then performed in mice expressing GCaMP3 in *Emx1*-lineage cells (Fig. 6*B*). Under N_2O anesthesia, network activity occurred in the form of spatiotemporal clusters of CaTs, frequently recruiting large parts of the FOV (~0.6 mm^2, $n = 22$; Fig. 6 *B–E*). Simultaneous LFP recordings revealed that approximately two-thirds of Ca^{2+} clusters were temporally unrelated to SPWs (−SPW; Fig. 6 *C–E* and *G* and *SI Appendix*). About one-fourth of −SPW-related LFP epochs had a relative beta (12 to 30 Hz) power significantly higher than that of cluster-free LFP periods (*SI Appendix*, Fig. S6*D* and #S18 in Table S6), suggesting that HNOs and −SPW Ca^{2+} clusters constitute partially overlapping event classes. However, most −SPW-related LFP epochs either lacked a clear electrophysiological signature or displayed inconsistent LFP changes different from SPWs (Fig. 6 *C–E* and *SI Appendix*, Fig. S6*D*). Of note, many beta-negative −SPW Ca^{2+} clusters were spatially confined and did not overlap with the LFP electrode (*SI Appendix*, Fig. S6*D*). In vivo two-photon Ca^{2+} imaging in WT mice revealed that only 13.1 ± 1.0% of somatic CaTs in CA1 PCs cooccurred with SPWs. Moreover, 14.2 ± 0.8% of CaTs followed SPWs with short (<3 s) latency, presumably reflecting SPW tails (16), whereas 72.8 ± 1.2% of CaTs were temporally unrelated to SPWs (*SI Appendix*, Fig. S6 *G–I*). Importantly, wide-field imaging confirmed that both +SPW and −SPW Ca^{2+} clusters were entirely AP dependent (*SI Appendix*, Fig. S6 *E* and *F*).

For quantification of Ca^{2+} imaging data, the FOV was subdivided into a regular grid of regions of interest (ROIs) (Fig. 6*B*). We found that the mean frequency of spontaneous CaTs per ROI was significantly lower in KO^{Emx1} mice than in WT littermates (Fig. 6*F* and *SI Appendix*, Table S6). Likewise, Ca^{2+}

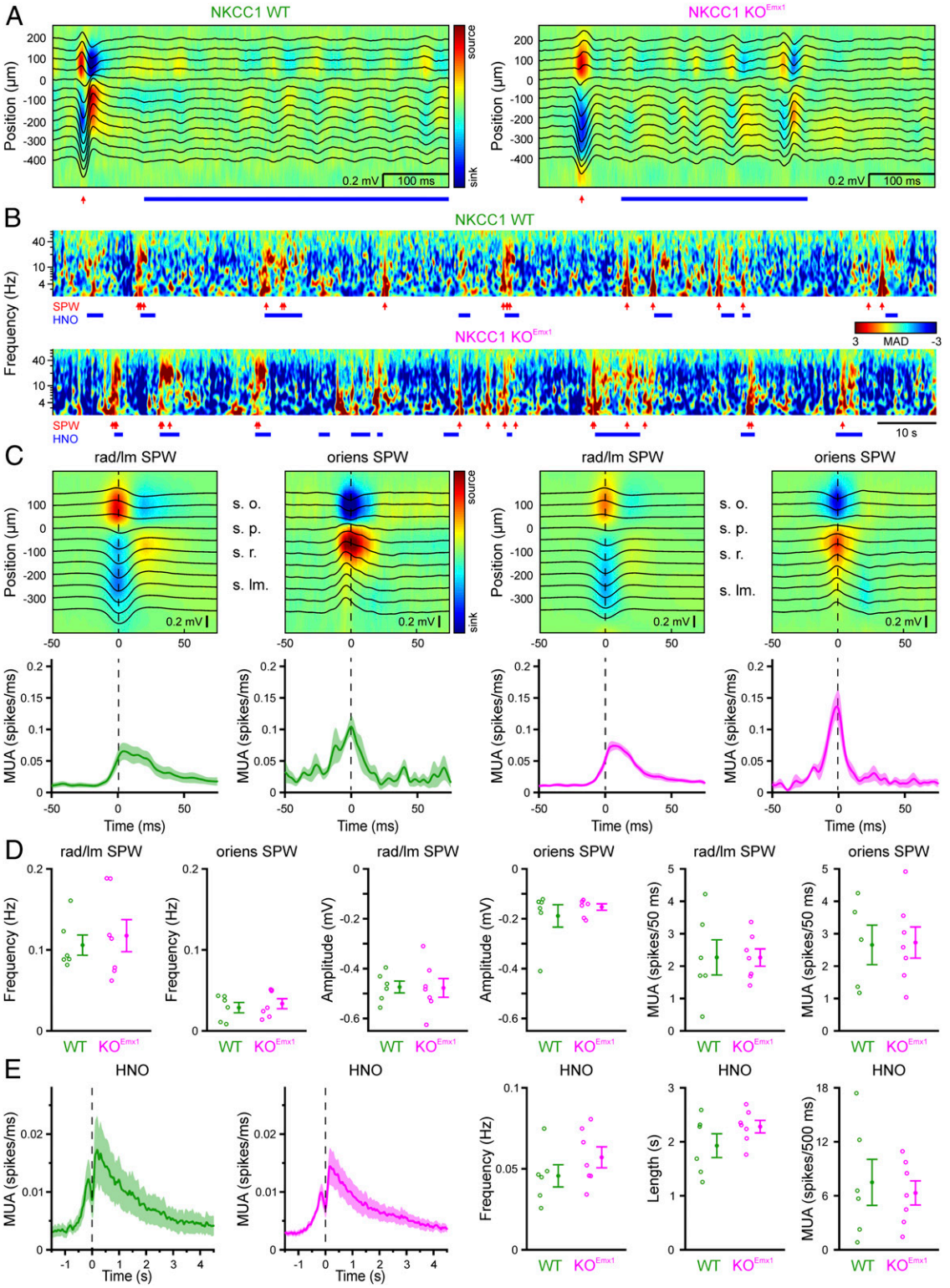

Fig. 5. Hippocampal sharp waves in vivo at P4 persist in NKCC1 KO^{Emx1} mice. (*A*) Example SPW (red arrow) and beta-frequency (~10- to 30-Hz range) hippocampal network oscillation (HNO, blue line) recorded by linear silicon probes. LFP traces (black) are superimposed over the current source density (CSD). 0 μm represents the field reversal of s.p. (*B*) Example wavelet spectrograms of CSD in s.l.m. in median absolute deviation (MAD) units per frequency. Events marked as in *A* and *B*. Note that some HNOs identified in the LFP may be of too small amplitude to be clearly visible in the wavelet of the CSD. (*C*) Median LFP and CSD depicted from SPWs with sinks either below ("rad/lm," *Left*) or above ("oriens," *Right*) s.p. *Left* two panels are from a WT, and *Right* two are from a KO^{Emx1} mouse. *Lower* panels display the SPW trough-aligned average MUA for all sets with five or more events. (*D*) Frequency, LFP amplitude, and MUA spike count of rad/lm and oriens SPWs. Displayed MUA counts are from 50-ms bins centered around the peak at 0 [−25, 25] ms for oriens SPWs, and after the peak from 0 [0, 50] ms for rad/lm SPWs. (*E*, *Left*) HNO start-aligned average MUA. Note the −200-ms peak in MUA due to (the ~30 to 60% of) HNO events having a preceding SPW (c.f. *A* and *B*). Note also that the MUA decay results from averaging HNOs of varying length. *Right* three panels, HNO occurrence rate, duration and MUA count in the [0, 500]-ms bin. Open circles represent single animals. Mean ± SEM. See *SI Appendix*, Fig. S5 and Table S5.

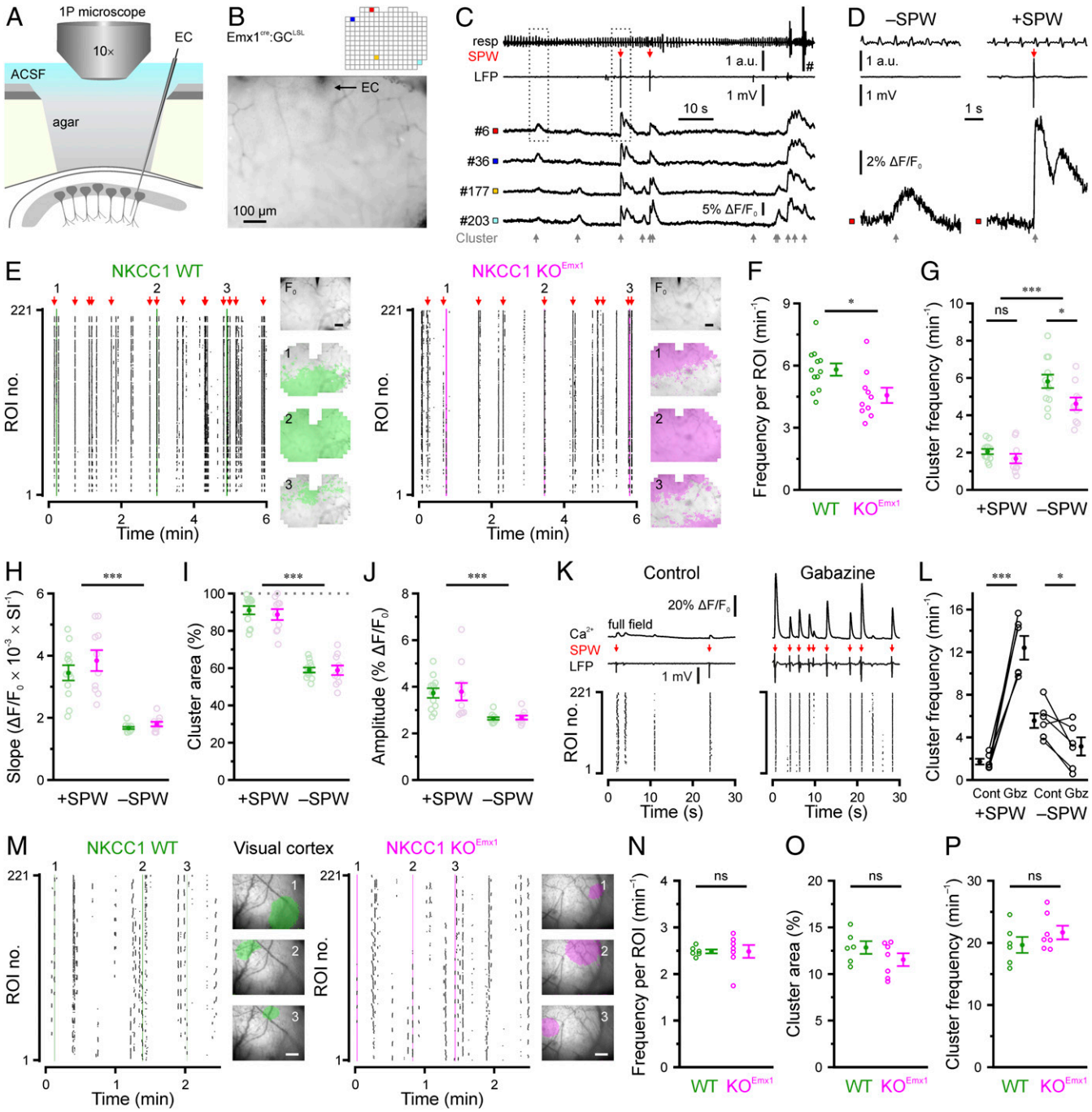

Fig. 6. NKCC1 promotes correlated network activity in an event type- and region-specific manner in vivo. (*A*) Experimental design. EC, extracellular electrode. (*B*) GCaMP fluorescence and ROIs for analysis. (*C*) Time-aligned GCaMP fluorescence (ROIs indicated in *B*), LFP (0.5 to 100 Hz) and respiration/movement (resp) signal. Ca^{2+} clusters are indicated by gray, SPWs by red arrows. Note CaTs with or without a concurrent SPW. (*D*) Boxed regions in *C* at higher magnification. +SPWs CaTs display faster rise kinetics and higher amplitudes. (*E*) Raster plots indicating CaT times per ROI. *Insets*: GCaMP fluorescence (F_0) and binary area plots of Ca^{2+} clusters indicated on the *Left*. (*F*) Reduced CaT frequencies per ROI. (*G*) $NKCC1^{Emx1}$ deletion reduced the frequency of –SPW Ca^{2+} clusters. (*H–J*) Rise kinetics (*H*), cluster area (*I*), and amplitude (*J*). SI, sampling interval. (*K*) Sample $\Delta F/F_0$ traces (mean of all analyzed ROIs), LFP (0.5 to 100 Hz), and raster plots before/after superfusion of gabazine (40 µM). Red arrows indicate detected SPWs (control) and SPW-like events (gabazine). (*L*) +SPW and –SPW Ca^{2+} cluster frequencies. (*M*) Sample raster plots demonstrating cluster activity in the visual neocortex. *Insets*: Transcranial GCaMP fluorescence overlaid with binary area plots of three events indicated on the *Left*. (Scale bars, 200 µm.) (*N–P*) Average CaT frequency per ROI (*N*), mean cluster area (*O*), and cluster frequency (*P*). Open circles represent single animals. Mean ± SEM; ns, not significant; $*P < 0.05$, $***P < 0.001$. See *SI Appendix*, Figs. S6–S8 and Table S6.

cluster frequency was reduced from 7.9 ± 0.4 min^{-1} in WT to 6.3 ± 0.4 min^{-1} in KO^{Emx1} mice (*SI Appendix*, #S2 in Table S6). Thus, our data identify an excitatory network effect of $NKCC1^{Emx1}$. While there was no significant interaction between the independent variables (genotype × SPW), the frequency of –SPW, but not of +SPW events was significantly reduced (Fig. 6*G*). The frequency of LFP-SPWs was not altered either, in line with the observation that >90% of SPWs resulted in a Ca^{2+} cluster (*SI Appendix*, #S3

in Table S6). As compared with +SPW Ca^{2+} clusters, −SPW events had slower rise kinetics (Fig. 6*H*), smaller cluster areas (Fig. 6*I*), and lower CaT amplitudes (Fig. 6*J*), pointing to a separate class of events. Interestingly, no genotype-dependent difference was found in any of these parameters (*SI Appendix*, #S4–S6 in Table S6), demonstrating that network dynamics in NKCC1 KO^{Emx1} mice qualitatively resembled those observed in WT mice.

Depolarizing GABA can mediate both excitation and inhibition in a context-dependent manner (47–49). We therefore examined the contribution of endogenously released GABA by locally blocking $GABA_A$Rs. Superfusion of the hippocampal window with gabazine (40 μM) induced a significant increase in LFP-SPW frequencies, amplitudes, and durations (*SI Appendix*, #S9–S11 in Table S6), indicating that SPW-like events in the presence of gabazine may be mechanistically different from SPWs in control. Furthermore, gabazine increased the frequency of +SPW Ca^{2+} clusters, but decreased that of −SPW events (Fig. 6 *K* and *L*). Additionally, amplitudes of both event classes increased following $GABA_A$R block, but this effect was significantly stronger for +SPW Ca^{2+} clusters (*SI Appendix*, #S8 in Table S6). Effects of $GABA_A$R inhibition on −SPW Ca^{2+} clusters were similar to those on network events in vitro, where gabazine (20 μM) induced a profound increase in amplitude, but not frequency (*SI Appendix*, Fig. S7 *A–D*). Collectively, our data suggest that GABA can facilitate −SPW Ca^{2+} clusters, while additionally imposing inhibitory constraints on spontaneous network activity.

Systemic application of the NKCC1 inhibitor bumetanide was previously found to abolish SPWs (35) or leave SPWs unaffected (36). Bypassing the blood–brain barrier (34), we aimed at blocking NKCC1 by superfusing the hippocampal window with bumetanide (50 μM) for a prolonged time period (60 min) (*SI Appendix*, Fig. S7*E*). Surprisingly, we observed moderate increases in the frequencies of CaTs as well as +SPW and −SPW Ca^{2+} clusters. These changes occurred in both genotypes (*SI Appendix*, Fig. S7 *F–H* and #S23–S25 in Table S6). While the activity increase might reflect cell-type-specific effects of NKCC1 and/or time-dependent alterations, this dataset supports the view that NKCC1 in PCs is not instrumental for SPW generation.

In contrast to our results in hippocampus, previous electrophysiological (36, 50) or optical (14) measurements did not reveal a contribution of NKCC1 to network activity in neocortex. As this might imply brain region-dependent differences in the role of NKCC1 and, thus, depolarizing GABA (33), we performed additional experiments in the visual cortex (P3 to 4). Cell-attached recordings in acute slices confirmed that puff-applied isoguvacine induced AP firing in PCs from WT, but not from KO^{Emx1} mice (*SI Appendix*, Fig. S8 *A–C*). Moreover, *Slc12a2* mRNA levels in the visual cortex of neonatal NKCC1 KO^{Emx1} mice were strongly reduced (*SI Appendix*, Fig. S8*D*). Using in vivo wide-field Ca^{2+} imaging, we found that spontaneous network activity was unaffected by NKCC1 loss at P3 to 4 (Fig. 6 *M–P*) and P9 to 10 (*SI Appendix*, Fig. S8 *E–H*). Furthermore, multisite LFP recordings revealed that spindle bursts, the main electrophysiological signature of Ca^{2+} clusters in the neonatal visual cortex (14), were unaltered in KO^{Emx1} mice (*SI Appendix*, Fig. S8 *I–K*).

Collectively, our data indicate that PC-specific expression of NKCC1 has a minor effect on in vivo correlated spontaneous activity (−SPW) in the hippocampus, whereas network activity in visual cortex is independent of NKCC1.

Long-Term Alterations of In Vivo Hippocampal Network Dynamics upon $NKCC1^{Emx1}$ Deletion. As correlated spontaneous activity contributes to the maturation of neuronal circuits (51, 52), we next investigated the long-term developmental effects of $NKCC1^{Emx1}$ deletion onto in vivo hippocampal network dynamics in urethane-anesthetized 13- to 14-wk-old mice. We recorded depth profiles of spontaneous LFPs along the CA1–dentate gyrus axis. Hippocampal LFPs from both WT and NKCC1 KO^{Emx1} mice showed paradoxical (rapid eye movement [REM]) sleep-like activity, i.e., theta/gamma oscillations and non-REM slow wave sleep (SWS)-like LFP epochs with the characteristic SPW-ripple (SPW-R) complexes in CA1. These activity patterns alternated spontaneously throughout the recording session (Fig. 7*A*). LFP analysis of theta power depth profiles during REM-like epochs with similar theta phase depth profiles (*SI Appendix*, Fig. S9 *A* and *B*) revealed increased theta amplitudes in stratum lacunosum moleculare (s.l.m.) and stratum moleculare (s.m.), whereas amplitudes of low-gamma and MUA frequency bands were unaffected (Fig. 7 *B* and *C* and *SI Appendix*, Table S7). Analysis of SPW-Rs during SWS-like LFP epochs revealed lower ripple spectral frequencies, unchanged SPW amplitudes, and decreased occurrence rates (Fig. 7*D*). Cross-frequency coupling between theta and gamma oscillations, i.e., the modulation of gamma amplitudes by theta phase, was unaltered in KO^{Emx1} mice (*SI Appendix*, Fig. S9 *C* and *D*). In addition, peak spectral frequencies in the theta (3 to 7 Hz) or gamma (30 to 100 Hz) range were similar in both genotypes (*SI Appendix*, Fig. S9*E*). Together, our data indicate that NKCC1 deletion from forebrain PCs altered the properties of theta oscillations in hippocampal layers receiving entorhinal input as well as intrahippocampal dynamics during ripple oscillations.

We further analyzed single-cell network dynamics using two-photon Ca^{2+} imaging in s.p. at P45 to 50 under isoflurane anesthesia (Fig. 7*E*). As previously reported (53), CaT frequency distributions were strongly skewed to the right in either genotype (Fig. 7 *F* and *G*). Moreover, mean CaT frequencies did not differ significantly between WT and KO^{Emx1} mice (Fig. 7*H*). Based on pairwise Pearson correlations we found that, by the age investigated, CA1 network activity had transitioned to a largely desynchronized state in both genotypes (54). Quantitatively, however, Pearson correlations were significantly lower in KO^{Emx1} mice (Fig. 7 *I* and *J*). Likewise, the spike-time tiling coefficient, an independent affinity metric (55), was significantly lower in the conditional absence of NKCC1 (Fig. 7*K*). These differences were abolished by randomly shuffling CaT times, confirming that they had not arisen from an inequality of CaT frequencies.

Collectively, our data demonstrate subtle long-term alterations in both intrahippocampal dynamics and entorhinal cortex–hippocampus communication due to PC-specific NKCC1 deletion.

Discussion

NKCC1 Dependency of Network Dynamics In Vivo. NKCC1 mediates chloride accumulation in immature neurons, giving rise to a mainly depolarizing action of GABA in vivo (13–15). However, the in vivo network functions of NKCC1-dependent GABAergic depolarization remained elusive (reviewed in ref. 29). Conflictingly, systemic application of the NKCC1 inhibitor bumetanide was found to either abolish SPWs (35) or leave SPWs unaffected (36). Technical limitations of in vivo pharmacological approaches, as of local application used here (*SI Appendix*, Fig. S7 *E–H*), include the lack of cell-type specificity and poor concentration control. By conditionally deleting *Slc12a2* from telencephalic glutamatergic cells, we overcome these limitations and demonstrate that NKCC1 facilitates synchronized network activity in the neonatal CA1 in vivo. Specifically, NKCC1 deletion selectively reduced the frequency of −SPW Ca^{2+} clusters (by ∼20%), while SPWs were unaffected (Figs. 5 and 6). Developmental compensations cannot be excluded from our data, including those that act at the level of $[Cl^-]_i$ and/or $[HCO_3^-]_i$ (10, 56, 57). However, if the latter are present at all, they are partial, as we demonstrate that NKCC1 shifted E_{GABA} by on average ∼8 mV in hippocampal slices. As our transgenic approach ensures that the manipulation of NKCC1 is equally operative in slices and intact brains, our data point to a differential impact of NKCC1 in vivo vs. in vitro. Additionally, no compensatory alterations in intrinsic/synaptic properties were detected in NKCC1 KO^{Emx1} mice that could explain the observed minor effect on network dynamics in vivo. Moreover,

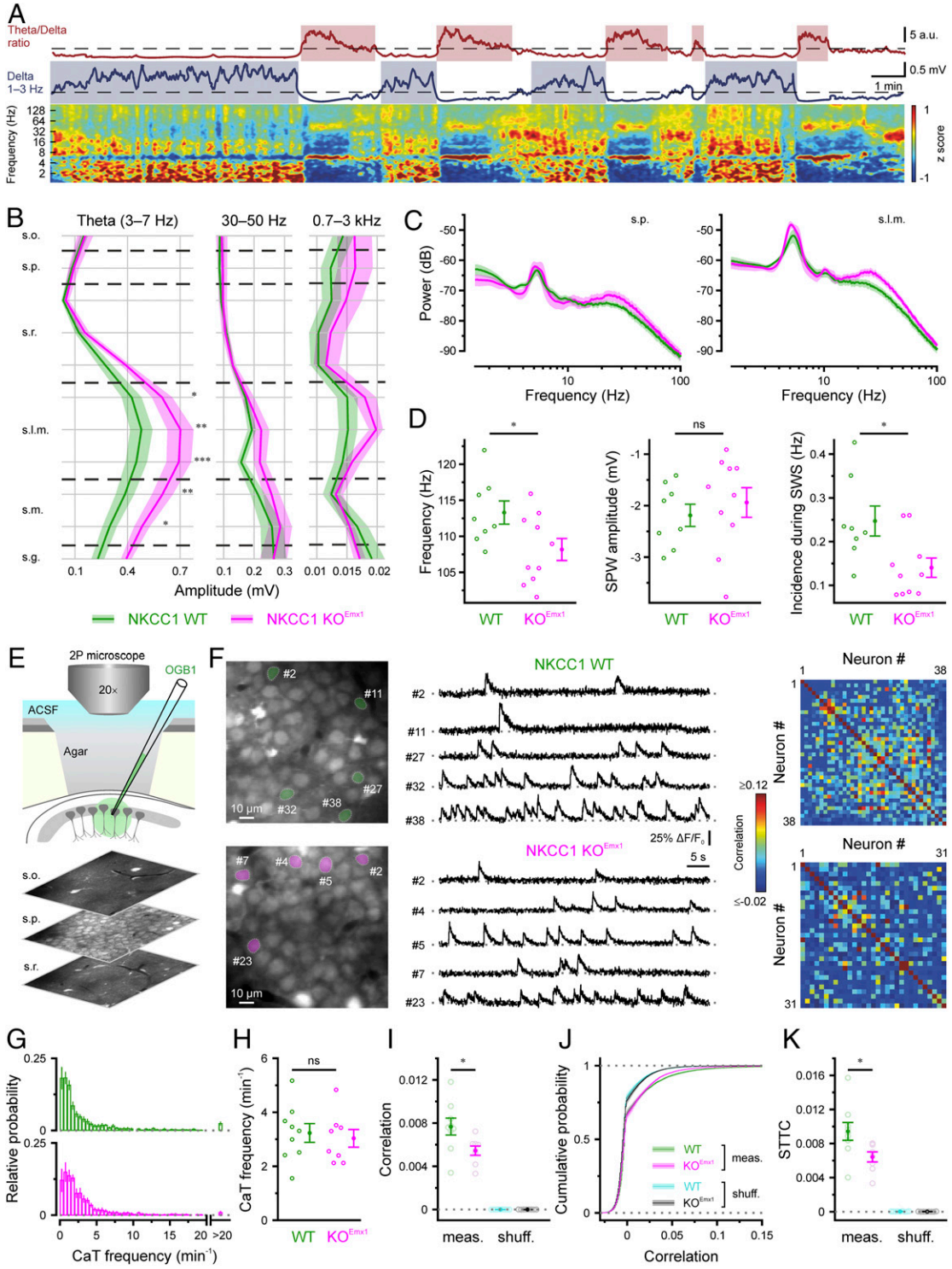

Fig. 7. Long-term alterations of in vivo hippocampal network dynamics upon NKCC1^{Emx1} deletion. (*A*) *Top*: Representative example of REM- and SWS-like activity classification of the hippocampal LFP in adult urethane-anesthetized mice. SWS- and REM-like activity in s.l.m. showed characteristic inverted peaks in the delta band (blue) and theta/delta ratio (red), respectively. *Bottom*: Z-score normalized wavelet spectrogram showing differences in theta and delta power between REM- and SWS-like oscillations. (*B*) Band-limited power analysis during REM-like activity. Theta amplitude (*Left*) in s.l.m. and s.m. was higher in KO^{Emx1} compared with WT mice. Low-gamma (*Middle*) and MUA (0.7 to 3 kHz, *Right*) frequency bands were unaffected, as were the remaining frequency bands analyzed (see *SI Appendix*). Shaded areas represent ± SEM across animals. (*C*) Power spectra from s.p. and s.l.m. (*D*) SPW-R events occurring during SWS-like activity showed lower spectral frequency (*Left*) and incidence (*Right*) in KO^{Emx1} mice. Ripple-associated SPWs showed no significant amplitude difference between the genotypes (*Middle*). (*E*) Experimental arrangement and sample OGB1 fluorescence images. (*F*, *Left*) Two-photon fluorescence images; (*F*, *Middle*) sample $\Delta F/F_0$ traces; (*F*, *Right*) Pearson correlation matrices for the same FOVs. (*G*) Single-cell CaT frequencies (averaged across animals). (*H*) Mean CaT frequencies. (*I*) Mean pairwise Pearson correlation coefficients for measured and randomly shuffled CaT trains. (*J*) Distributions of Pearson correlation coefficients. (*K*) Mean spike-time tiling coefficients (STTC) for measured data and randomly shuffled CaT trains. Open circles represent single animals. Mean ± SEM; ns, not significant; $*P < 0.05$, $**P < 0.01$, $***P < 0.001$. See *SI Appendix*, Fig. S9 and Table S7.

the impact of NKCC1 is region specific, as its deletion failed to affect spindle bursts in the visual cortex. Conceptually, this conclusion is supported by a recent chemogenetic study revealing that GABA is excitatory in CA1, but inhibitory in V1 (33). Mechanisms underlying this region specificity are unknown, but it is worth noting that NKCC1 did contribute to the maintenance of GABAergic excitation in both CA1 (Fig. 2) and V1 (*SI Appendix*, Fig. S8) in vitro.

The +SPW and −SPW Ca^{2+} clusters were differentially modulated by local $GABA_AR$ inhibition, as gabazine increased the frequency of +SPW Ca^{2+} clusters, but decreased that of −SPW events (Fig. 6*L*). This observation might explain discrepant results of two well-designed recent studies, in which either inhibitory (25) or excitatory (33) GABA effects were found to dominate. Hence, we argue that $GABA_AR$ signaling has a dual (excitatory–inhibitory) role in the neonatal CA1. Which mechanism(s) could underlie the excitatory vs. inhibitory GABA effects at this age? GABAergic depolarization may either increase or decrease neuronal firing—depending on the $GABA_AR$ conductance, E_{GABA}, and the spatiotemporal patterning of synaptic inputs (47–49). Spindle bursts and SPWs are driven by synchronized inputs from the lateral geniculate nucleus (18) and entorhinal cortex (45), respectively, while our LFP data suggest that this may not be the case with −SPW events. Though speculative, such differences in synaptic inputs might explain why −SPW Ca^{2+} clusters are NKCC1 dependent, whereas spindle bursts and SPWs are not. Whether different classes of GABAergic interneurons (58) serve differential functions in vivo, remains unknown.

Two Classes of Network Events in the Neonatal CA1 In Vivo. Employing Ca^{2+} imaging with LFP recordings, we identified two classes of network events in the neonatal CA1: +SPW and −SPW Ca^{2+} clusters, which differed in several basic parameters (Fig. 6 *H–J*). As compared with neonatal V1 (18, 19), CA1 Ca^{2+} clusters were less spatially confined. This was most prominent for +SPW events, which tended to activate the entire FOV (59) and frequently followed myoclonic limb/body twitches (45, 60) (*SI Appendix*, Fig. S6*C*). Thus, SPWs may provide a pan-CA1 input signal representing, e.g., somatosensory feedback. Of note, −SPW events, of which one-fourth had a significant beta power, constituted about two-thirds of all Ca^{2+} clusters detected at P3 to 4 (Fig. 6*G*). Since GCaMP signals mainly reflect neuronal firing (61), our data indicate that a considerable fraction of APs in CA1 PCs is not driven by SPWs (45). This conclusion is supported by two-photon Ca^{2+} imaging (*SI Appendix*, Fig. S6 *G–I*) and electrophysiological data from freely moving rat pups (P4 to 6) showing that ∼60% of CA1 MUA bursts were not associated with SPWs (16). Some −SPW Ca^{2+} clusters followed +SPW events with short delays and, hence, might reflect SPW tails (Fig. 5*E*) (16, 36). Given their descriptive differences and differential dependence on NKCC1 (Figs. 5 and 6*G*) and $GABA_AR$ signaling (Fig. 6*L*), we argue that +SPW and −SPW events are mechanistically distinct. Based on their differential kinetics and NKCC1 dependence, we further propose that GDPs do not represent the in vitro analog of SPWs recorded in vivo. We revealed that GDPs share pharmacological properties with −SPW events, as both are NKCC1 dependent and disinhibited in amplitude, but not frequency, by gabazine. Given that GDPs are generated in CA1 even if deafferented from CA3 and cortical inputs (62), it is tempting to speculate that −SPW Ca^{2+} clusters might emerge from and reflect a property of local intrahippocampal circuits, whereas SPW generation requires cortical input (45).

Developmental Functions of NKCC1-Dependent GABAergic Depolarization. We found that several passive and active (Fig. 4 *A–E*) membrane properties were unaffected by $NKCC1^{Emx1}$ loss. This suggests that compensatory changes in intrinsic excitability, observed in conventional NKCC1 mice (11) or after E15 to P7 pharmacological NKCC1 blockade (63), may be due to loss of NKCC1 function in other cell types, or reflect secondary alterations related to NKCC1 deletion outside the brain. Rigorous approaches will be required to clarify potential functions of NKCC1 in GABAergic interneurons. Furthermore, basic characteristics of AMPAR- and $GABA_AR$-mediated transmission were unaltered in NKCC1 KO^{Emx1} mice (Fig. 4 *F–I*). This challenges the hypothesis of the importance of NKCC1-dependent GABAergic depolarization as a universal requirement for the NMDAR-dependent developmental unsilencing of glutamatergic synapses (9, reviewed in refs. 29, 63)—although depolarizing GABA may facilitate NMDAR activation by attenuating their voltage-dependent Mg^{2+} block (64). Collectively, our data indicate that network effects induced by NKCC1 disruption in telencephalic PCs directly result from changes in E_{GABA} (i.e., $[Cl^-]_i$). Thus, we confirm previous in vitro (8, 12, 35) and recent in vivo (13–15) evidence indicating that NKCC1 maintains high $[Cl^-]_i$ in immature neurons. Of note, NKCC1 deletion did not completely abolish depolarizing responses to GABA in acute slices, suggesting that factors other than NKCC1 also contribute (10). Additionally, optical and electrophysiological measurements demonstrated subtle alterations of network dynamics in adult NKCC1 KO^{Emx1} mice (Fig. 7). Whether these changes reflect developmental adaptations or acute effects due to altered E_{GABA}, e.g., in the axon initial segment (65, 66), remains unknown. Importantly, they were not associated with performance deficits in hippocampus-dependent behavioral tasks (Fig. 1). These findings may be clinically relevant, as NKCC1 has emerged as a potential target for the treatment of neurodevelopmental disorders (36, 67, 68). While our study does not rule out more specific long-term developmental functions of NKCC1 and/or roles of NKCC1 under pathophysiological conditions, our data converge to suggest that basal physiological NKCC1 activity in telencephalic glutamatergic neurons is largely dispensable for several key aspects of cortical network maturation.

Materials and Methods

Animals. Mouse strains used in this study are listed in *SI Appendix*, Table S8. All animal procedures were performed with the approval of the local governments (Thüringer Landesamt für Verbraucherschutz, Bad Langensalza, Germany, and Landesamt für Natur-, Umwelt- und Verbraucherschutz, NRW, Recklinghausen, Germany) and complied with European Union norms (Directive 2010/63/EU). *Emx1*^{IREScre} (#005628), *GCaMP3*^{LSL} (Ai38, #014538), *GCaMP6s*^{LSL} (Ai96, #024106), *tdTomato*^{LSL} (Ai14, #007908), and C57BL/6J (#000664) mice were originally obtained from The Jackson Laboratory. *NKCC1*^{flox} (*Slc12a2*^{flox}) mice were generated as previously described (38). The age of the animals is indicated in *Results*. Mice of either sex were used. Experiments were performed blinded to genotype. Further details are provided in *SI Appendix*.

Electrophysiological, Optical, and Behavioral Experiments. A description of all experimental and analytical procedures is provided in *SI Appendix*.

Statistical Analysis. Unless otherwise stated, the statistical parameter *n* refers to the number of 1) animals for in vivo experiments, 2) slices for in vitro Ca^{2+} imaging, and 3) cells in patch-clamp recordings, respectively. All data are reported as mean ± SEM, if not stated otherwise. The Kolmogorov–Smirnov test or Shapiro–Wilk test was used to test for normality. Parametric testing procedures were applied for normally distributed data; otherwise nonparametric tests were used. In the case of two-sample *t* tests and unequal group variances, Welch's correction was applied. For multigroup comparisons, ANOVA was applied. Analysis of covariance (ANCOVA) was used to control for covariate effects. *P* values (two-tailed tests) <0.05 were considered statistically significant. Details of the statistical tests applied are provided in *SI Appendix*, Tables S1–S7.

Data Availability. All data discussed in the paper are available in the main text and *SI Appendix*.

ACKNOWLEDGMENTS. We thank Ina Ingrisch and Sindy Beck for excellent technical assistance and Dr. John Dempster (University of Strathclyde, Glasgow) for adapting WinFluor. This work was supported by grants from the Priority Program 1665 (HO 2156/3–1/2 to K.H., KI 1816/1–1/2 to K.K., KI 1638/3–1/2 to S.J.K., IS63/5–1 to D.I., and HU 800/8–1/2 to C.A.H.); the

Collaborative Research Center/Transregio 166 (B3 to K.H. and K.K.); the Collaborative Research Center 1089 (A05 to D.I. and S.L.M.); the Research Unit 3004 (KI 1816/5-1 to K.K.); the Research Unit 2715 (IS63/10-1 to D.I.); and individual grants (KI 1816/6-1 and KI 1816/7-1 to K.K., HO 2156/5-1, HO 2156/6-1 to K.H., and 449505290 to T.F.) of the German Research Foundation, the Federal Ministry of Education and Research (NEURON ACRoBAT to C.A.H., 01GQ0923 to K.H. and O.W.W.), and the Interdisciplinary Centre for Clinical Research Jena (A.U., K.K., and K.H.).

1. J. Bormann, O. P. Hamill, B. Sakmann, Mechanism of anion permeation through channels gated by glycine and gamma-aminobutyric acid in mouse cultured spinal neurones. *J. Physiol.* **385**, 243–286 (1987).
2. C. Rivera *et al*., The K+/Cl- co-transporter KCC2 renders GABA hyperpolarizing during neuronal maturation. *Nature* **397**, 251–255 (1999).
3. N. Doyon, L. Vinay, S. A. Prescott, Y. De Koninck, Chloride regulation: A dynamic equilibrium crucial for synaptic inhibition. *Neuron* **89**, 1157–1172 (2016).
4. K. Krnjevic, J. W. Phillis, Iontophoretic studies of neurones in the mammalian cerebral cortex. *J. Physiol.* **165**, 274–304 (1963).
5. K. Allen, H. Monyer, Interneuron control of hippocampal oscillations. *Curr. Opin. Neurobiol.* **31**, 81–87 (2015).
6. H. J. Luhmann, D. A. Prince, Postnatal maturation of the GABAergic system in rat neocortex. *J. Neurophysiol.* **65**, 247–263 (1991).
7. A. Spoljaric *et al*., Vasopressin excites interneurons to suppress hippocampal network activity across a broad span of brain maturity at birth. *Proc. Natl. Acad. Sci. U.S.A.* **114**, E10819–E10828 (2017).
8. J. Yamada *et al*., Cl- uptake promoting depolarizing GABA actions in immature rat neocortical neurones is mediated by NKCC1. *J. Physiol.* **557**, 829–841 (2004).
9. D. D. Wang, A. R. Kriegstein, GABA regulates excitatory synapse formation in the neocortex via NMDA receptor activation. *J. Neurosci.* **28**, 5547–5558 (2008).
10. C. K. Pfeffer *et al*., NKCC1-dependent GABAergic excitation drives synaptic network maturation during early hippocampal development. *J. Neurosci.* **29**, 3419–3430 (2009).
11. S. T. Sipilä *et al*., Compensatory enhancement of intrinsic spiking upon NKCC1 disruption in neonatal hippocampus. *J. Neurosci.* **29**, 6982–6988 (2009).
12. V. I. Dzhala *et al*., NKCC1 transporter facilitates seizures in the developing brain. *Nat. Med.* **11**, 1205–1213 (2005).
13. S. Sulis Sato *et al*., Simultaneous two-photon imaging of intracellular chloride concentration and pH in mouse pyramidal neurons in vivo. *Proc. Natl. Acad. Sci. U.S.A.* **114**, E8770–E8779 (2017).
14. K. Kirmse *et al*., GABA depolarizes immature neurons and inhibits network activity in the neonatal neocortex in vivo. *Nat. Commun.* **6**, 7750 (2015).
15. J. J. van Rheede, B. A. Richards, C. J. Akerman, Sensory-evoked spiking behavior emerges via an experience-dependent plasticity mechanism. *Neuron* **87**, 1050–1062 (2015).
16. X. Leinekugel *et al*., Correlated bursts of activity in the neonatal hippocampus in vivo. *Science* **296**, 2049–2052 (2002).
17. R. Khazipov *et al*., Early motor activity drives spindle bursts in the developing somatosensory cortex. *Nature* **432**, 758–761 (2004).
18. J. B. Ackman, T. J. Burbridge, M. C. Crair, Retinal waves coordinate patterned activity throughout the developing visual system. *Nature* **490**, 219–225 (2012).
19. M. Kummer *et al*., Column-like Ca(2+) clusters in the mouse neonatal neocortex revealed by three-dimensional two-photon Ca(2+) imaging in vivo. *Neuroimage* **138**, 64–75 (2016).
20. T. Arichi *et al*., Localization of spontaneous bursting neuronal activity in the preterm human brain with simultaneous EEG-fMRI. *eLife* **6**, e27814 (2017).
21. O. Blanquie *et al*., Electrical activity controls area-specific expression of neuronal apoptosis in the mouse developing cerebral cortex. *eLife* **6**, e27696 (2017).
22. W. C. Oh, S. Lutzu, P. E. Castillo, H. B. Kwon, De novo synaptogenesis induced by GABA in the developing mouse cortex. *Science* **353**, 1037–1040 (2016).
23. J. Zhang, J. B. Ackman, H. P. Xu, M. C. Crair, Visual map development depends on the temporal pattern of binocular activity in mice. *Nat. Neurosci.* **15**, 298–307 (2011).
24. J. Winnubst, J. E. Cheyne, D. Niculescu, C. Lohmann, Spontaneous activity drives local synaptic plasticity in vivo. *Neuron* **87**, 399–410 (2015).
25. G. Valeeva, T. Tressard, M. Mukhtarov, A. Baude, R. Khazipov, An optogenetic approach for investigation of excitatory and inhibitory network GABA actions in mice expressing channelrhodopsin-2 in GABAergic neurons. *J. Neurosci.* **36**, 5961–5973 (2016).
26. J. C. Wester, C. J. McBain, Interneurons differentially contribute to spontaneous network activity in the developing Hippocampus dependent on their embryonic lineage. *J. Neurosci.* **36**, 2646–2662 (2016).
27. T. Flossmann *et al*., Somatostatin interneurons promote neuronal synchrony in the neonatal Hippocampus. *Cell Rep.* **26**, 3173–3182.e5 (2019).
28. S. Rheims *et al*., Excitatory GABA in rodent developing neocortex in vitro. *J. Neurophysiol.* **100**, 609–619 (2008).
29. K. Kirmse, C. A. Hübner, D. Isbrandt, O. W. Witte, K. Holthoff, GABAergic transmission during brain development: Multiple effects at multiple stages. *Neuroscientist* **24**, 36–53 (2018).
30. B. Han, A. Bellemer, M. R. Koelle, An evolutionarily conserved switch in response to GABA affects development and behavior of the locomotor circuit of Caenorhabditis elegans. *Genetics* **199**, 1159–1172 (2015).
31. M. T. Colonnese *et al*., A conserved switch in sensory processing prepares developing neocortex for vision. *Neuron* **67**, 480–498 (2010).
32. A. Che *et al*., Layer I interneurons sharpen sensory maps during neonatal development. *Neuron* **99**, 98–116.e7 (2018).
33. Y. Murata, M. T. Colonnese, GABAergic interneurons excite neonatal hippocampus in vivo. *Sci. Adv.* **6**, eaba1430 (2020).
34. W. Löscher, M. Puskarjov, K. Kaila, Cation-chloride cotransporters NKCC1 and KCC2 as potential targets for novel antiepileptic and antiepileptogenic treatments. *Neuropharmacology* **69**, 62–74 (2013).
35. S. T. Sipilä, S. Schuchmann, J. Voipio, J. Yamada, K. Kaila, The cation-chloride cotransporter NKCC1 promotes sharp waves in the neonatal rat hippocampus. *J. Physiol.* **573**, 765–773 (2006).
36. S. L. Marguet *et al*., Treatment during a vulnerable developmental period rescues a genetic epilepsy. *Nat. Med.* **21**, 1436–1444 (2015).
37. E. Delpire, J. Lu, R. England, C. Dull, T. Thorne, Deafness and imbalance associated with inactivation of the secretory Na-K-2Cl co-transporter. *Nat. Genet.* **22**, 192–195 (1999).
38. M. W. Antoine, C. A. Hübner, J. C. Arezzo, J. M. Hébert, A causative link between inner ear defects and long-term striatal dysfunction. *Science* **341**, 1120–1123 (2013).
39. L. Zhu, N. Polley, G. C. Mathews, E. Delpire, NKCC1 and KCC2 prevent hyperexcitability in the mouse hippocampus. *Epilepsy Res.* **79**, 201–212 (2008).
40. C. Zhang *et al*., Optimized photo-stimulation of halorhodopsin for long-term neuronal inhibition. *BMC Biol.* **17**, 95 (2019).
41. Y. Ben-Ari, E. Cherubini, R. Corradetti, J. L. Gaiarsa, Giant synaptic potentials in immature rat CA3 hippocampal neurones. *J. Physiol.* **416**, 303–325 (1989).
42. E. A. Stubblefield, T. A. Benke, Distinct AMPA-type glutamatergic synapses in developing rat CA1 hippocampus. *J. Neurophysiol.* **104**, 1899–1912 (2010).
43. A. S. Cohen, D. D. Lin, D. A. Coulter, Protracted postnatal development of inhibitory synaptic transmission in rat hippocampal area CA1 neurons. *J. Neurophysiol.* **84**, 2465–2476 (2000).
44. W. Fazeli *et al*., Early-life exposure to caffeine affects the construction and activity of cortical networks in mice. *Exp. Neurol.* **295**, 88–103 (2017).
45. G. Valeeva *et al*., Emergence of coordinated activity in the developing entorhinal-hippocampal network. *Cereb. Cortex* **29**, 906–920 (2019).
46. A. Mizrahi, J. C. Crowley, E. Shtoyerman, L. C. Katz, High-resolution in vivo imaging of hippocampal dendrites and spines. *J. Neurosci.* **24**, 3147–3151 (2004).
47. S. N. Kolbaev, K. Achilles, H. J. Luhmann, W. Kilb, Effect of depolarizing GABA(A)-mediated membrane responses on excitability of Cajal-Retzius cells in the immature rat neocortex. *J. Neurophysiol.* **106**, 2034–2044 (2011).
48. C. Jean-Xavier, G. Z. Mentis, M. J. O'Donovan, D. Cattaert, L. Vinay, Dual personality of GABA/glycine-mediated depolarizations in immature spinal cord. *Proc. Natl. Acad. Sci. U.S.A.* **104**, 11477–11482 (2007).
49. K. Morita, K. Tsumoto, K. Aihara, Bidirectional modulation of neuronal responses by depolarizing GABAergic inputs. *Biophys. J.* **90**, 1925–1938 (2006).
50. M. Minlebaev, Y. Ben-Ari, R. Khazipov, Network mechanisms of spindle-burst oscillations in the neonatal rat barrel cortex in vivo. *J. Neurophysiol.* **97**, 692–700 (2007).
51. S. Kirischuk *et al*., Modulation of neocortical development by early neuronal activity: Physiology and pathophysiology. *Front. Cell. Neurosci.* **11**, 379 (2017).
52. A. H. Leighton, C. Lohmann, The wiring of developing sensory circuits-from patterned spontaneous activity to synaptic plasticity mechanisms. *Front. Neural Circuits* **10**, 71 (2016).
53. M. A. Busche *et al*., Critical role of soluble amyloid-β for early hippocampal hyperactivity in a mouse model of Alzheimer's disease. *Proc. Natl. Acad. Sci. U.S.A.* **109**, 8740–8745 (2012).
54. N. L. Rochefort *et al*., Sparsification of neuronal activity in the visual cortex at eye-opening. *Proc. Natl. Acad. Sci. U.S.A.* **106**, 15049–15054 (2009).
55. C. S. Cutts, S. J. Eglen, Detecting pairwise correlations in spike trains: An objective comparison of methods and application to the study of retinal waves. *J. Neurosci.* **34**, 14288–14303 (2014).
56. E. Ruusuvuori *et al*., Carbonic anhydrase isoform VII acts as a molecular switch in the development of synchronous gamma-frequency firing of hippocampal CA1 pyramidal cells. *J. Neurosci.* **24**, 2699–2707 (2004).
57. A. T. Piala *et al*., Chloride sensing by WNK1 involves inhibition of autophosphorylation. *Sci. Signal.* **7**, ra41 (2014).
58. K. A. Pelkey *et al*., Hippocampal GABAergic inhibitory interneurons. *Physiol. Rev.* **97**, 1619–1747 (2017).
59. G. Valeeva, V. Rychkova, D. Vinokurova, A. Nasretdinov, R. Khazipov, Early sharp wave synchronization along the septo-temporal axis of the neonatal rat hippocampus. *Neurosci. Behav. Physiol.* **50**, 1195–1202 (2020).
60. K. A. Karlsson, E. J. Mohns, G. V. di Prisco, M. S. Blumberg, On the co-occurrence of startles and hippocampal sharp waves in newborn rats. *Hippocampus* **16**, 959–965 (2006).
61. J. N. Kerr, D. Greenberg, F. Helmchen, Imaging input and output of neocortical networks in vivo. *Proc. Natl. Acad. Sci. U.S.A.* **102**, 14063–14068 (2005).
62. L. Menendez de la Prida, S. Bolea, J. V. Sanchez-Andres, Origin of the synchronized network activity in the rabbit developing hippocampus. *Eur. J. Neurosci.* **10**, 899–906 (1998).
63. D. D. Wang, A. R. Kriegstein, Blocking early GABA depolarization with bumetanide results in permanent alterations in cortical circuits and sensorimotor gating deficits. *Cereb. Cortex* **21**, 574–587 (2011).
64. X. Leinekugel, I. Medina, I. Khalilov, Y. Ben-Ari, R. Khazipov, Ca2+ oscillations mediated by the synergistic excitatory actions of GABA(A) and NMDA receptors in the neonatal hippocampus. *Neuron* **18**, 243–255 (1997).
65. S. Khirug *et al*., GABAergic depolarization of the axon initial segment in cortical principal neurons is caused by the Na-K-2Cl cotransporter NKCC1. *J. Neurosci.* **28**, 4635–4639 (2008).
66. R. Tyzio *et al*., Postnatal changes in somatic gamma-aminobutyric acid signalling in the rat hippocampus. *Eur. J. Neurosci.* **27**, 2515–2528 (2008).
67. G. Deidda *et al*., Reversing excitatory GABAAR signaling restores synaptic plasticity and memory in a mouse model of Down syndrome. *Nat. Med.* **21**, 318–326 (2015).
68. R. Tyzio *et al*., Oxytocin-mediated GABA inhibition during delivery attenuates autism pathogenesis in rodent offspring. *Science* **343**, 675–679 (2014).